Pump it up

Luc Maffli[*a], Benjamin O'Brien[b], Samuel Rosset[a], Herbert Shea[a]

[a]Microsystems for Space Technologies Laboratory (LMTS), Ecole Polytechnique Fédérale de Lausanne (EPFL), Neuchâtel, Switzerland
[b]Biomimetics Laboratory, Bioengineering Institute, University of Auckland, New Zealand

ABSTRACT

We report on the use of zipping actuation applied to dielectric elastomer actuators to microfabricate mm-sized pumps. The zipping actuators presented here use electrostatic attraction to deform an elastomeric membrane by pulling it into contact with a rigid counter electrode. We present several actuation schemes using either conventional DEA actuation, zipping, or a combination of both in order to realize microfluidic devices. A zipping design in which the electric field is applied across the elastomer membrane was explored theoretically and experimentally. Single zipping chambers and a micropump body made of a three chambers connected by an embedded channel were wet-etched into a silicon wafer and subsequently covered by a gold-implanted silicone membrane. We measured static deflections of up to 300 μm on chambers with square openings of 1.8 and 2.6 mm side, in very good agreement with our model.

Keywords: Electro Active Polymers, Dielectric Elastomer Actuators, microfluidics, zipping, microfabrication, micropump, PDMS, KOH, Au ion implantation

1. INTRODUCTION

1.1. Dielectric Elastomer Actuators (DEAs) for microfluidics

DEAs are well-known for their large strains and energy densities comparable to piezo and magnetic actuators [1]. Their basic structure consists in two compliant electrodes patterned on both sides of a thin elastomer membrane. If a high electric field is applied across the membrane in free boundary conditions, the membrane compresses in thickness and expands in-plane due to the incompressibility of the elastomers. The type of applications targeted by this technology is as wide as artificial muscles, soft robotics, single cell stretching or energy harvesting.

In parallel, the microfluidic world is developing rapidly. Aside from the favorable scaling effects on fluid handling and sample analysis, one of the ultimate goals of miniaturized fluidic systems is to bring a whole laboratory processing chain on a few square centimeters: Lab-On-Chips (LOC) [2]. However, the current LOCs require many heavy and power-consuming off-chip controls like pneumatics and liquid pumps and valves. If the user takes benefit from the large number of operations that can be done on a single chip, the increase in complexity requires more and more off-chip controls. The advantages of miniaturization are therefore questionable, because the small chip remains bound to the lab.

DEAs for microfluidics are a promising option to face this issue: thanks to their electrical actuation, it is possible to imagine portable units to operate chips with pumps and valves integrated into the active membrane. The advantage of DEAs toward their piezoelectric competitors is the combination of large stroke volumes and high output forces. Indeed, piezoelectric diaphragms achieve excellent pumping performances, but are very limited in term of maximal deformations. Multipurpose software-reconfigurable microfluidic chips composed of arrays of actuated chambers, also called Microfluidic Large-Scale Integrated (MLSI) chips [3] [4] [5], are devices for which the use of DEAs could be particularly relevant. A large family of MLSI chips uses as actuation unit a chamber with an embedded channel in which a membrane deflects down to the bottom to close it. The membrane pushes the liquid out in the channel and finally closes it like a valve (Figure 1). In most of the existing chips, this actuation is done pneumatically.

* Correspondence: luc.maffli@epfl.ch

Electroactive Polymer Actuators and Devices (EAPAD) 2012, edited by Yoseph Bar-Cohen,
Proc. of SPIE Vol. 8340, 83402Q · © 2012 SPIE · CCC code: 0277-786X/12/$18 · doi: 10.1117/12.914831

Downloaded from SPIE Digital Library on 18 Apr 2012 to 128.178.201.191. Terms of Use: http://spiedl.org/terms

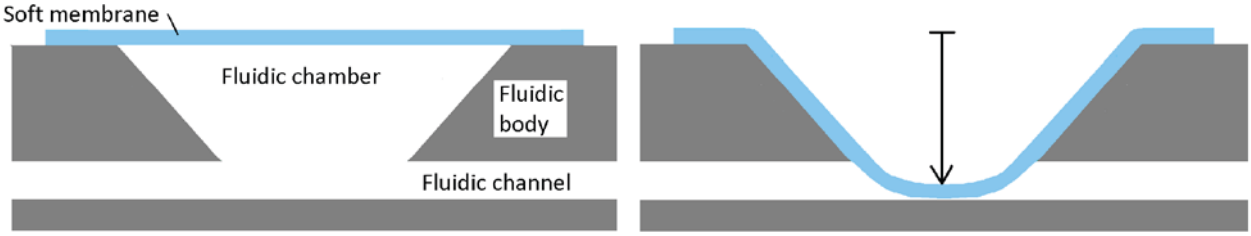

Figure 1
Basic MLSI chip unit in open (left) and closed state (right)

However, fluid handling with DEAs rises new issues such as the high driving voltages, thin membranes and the interaction of liquids and silicone actuators. The actuator should also deflect in a well-controlled manner, and toward the bottom of the chamber. For a structure like on Figure 1, the membrane must be able to seal the cavity. Thus, it is necessary to extend the traditional structure of DEAs to imagine new actuation principles. Ideally, they must meet the following challenges: keep the processed liquid at a floating or possibly grounded potential, avoid electric fields in it, prevent premature breakdown induced by the change in electrical properties of the membrane in contact with the liquid, ensure a leakage-free sealing of the fluidic features, make a conformal seal on the channel walls in deflected state, and guarantee the security of the user. Additionally, we expect that these new actuation principles will enhance the output force and the achievable strain of the actuators.

To produce work on fluids, an out-of plane motion of the actuator's membrane is required. The most suitable existing candidate would be the buckling DEA, which consists in a membrane fixed on a rigid aperture. Under application of the voltage, the in-plane strain is transferred to out-of plane buckling because of the fixed boundary conditions [6]. But considering the previously mentioned objectives, it is a poor candidate, because the membrane would not deflect against the walls of the chamber, but in a spherical shape. In addition, it could buckle in up- or downward direction.

One key to open the door to novel DEA structures is the use of electrostatic zipping, which is a well-known actuation method for silicon Micro Electro-Mechanical Systems (MEMS) [7]. Unlike "squeezing-mode" DEAs where the elastomer membrane is compressed by the electric field between two compliant electrodes, a soft electrode is attracted toward a fixed one. The dielectric across which the electric field is applied can either be the elastomer membrane, a solid layer deposited on the rigid electrode, or both [8] [9]. By applying the electric field across a few microns thick rigid dielectric with high breakdown strength, the actuation force at constant voltage is much greater than with silicone or acrylic elastomers. In our work, we adapt zipping to silicone membranes implanted with gold ions. These electrodes do not leave residues when they come in contact with a surface, are compatible with batch microfabrication processes and easily patternable with features as small as 50 μm.

1.2. Novel zipping geometries studied

A variety of new actuation structures for active fluidic chambers can be considered (Figure 2).

Structure A is a buckling DEA actuator [6] [10]. A non-prestretched membrane with two compliant electrodes covering the entire membrane's surface is bonded to a rigid frame. The application of a voltage makes the membrane buckle out of plane.

Solution B [11] is similar to A, but with the lower electrode replaced by a conductive liquid. It presents the advantage of great simplicity, since the lower electrode is the liquid itself. It is also easier to seal the channel by silicone to silicone or silicone to glass bonding of the membrane on the chip. Like for A, it does not have a preferential buckling direction, and does not offer a conformal chamber sealing.

Downloaded from SPIE Digital Library on 18 Apr 2012 to 128.178.201.191. Terms of Use: http://spiedl.org/terms

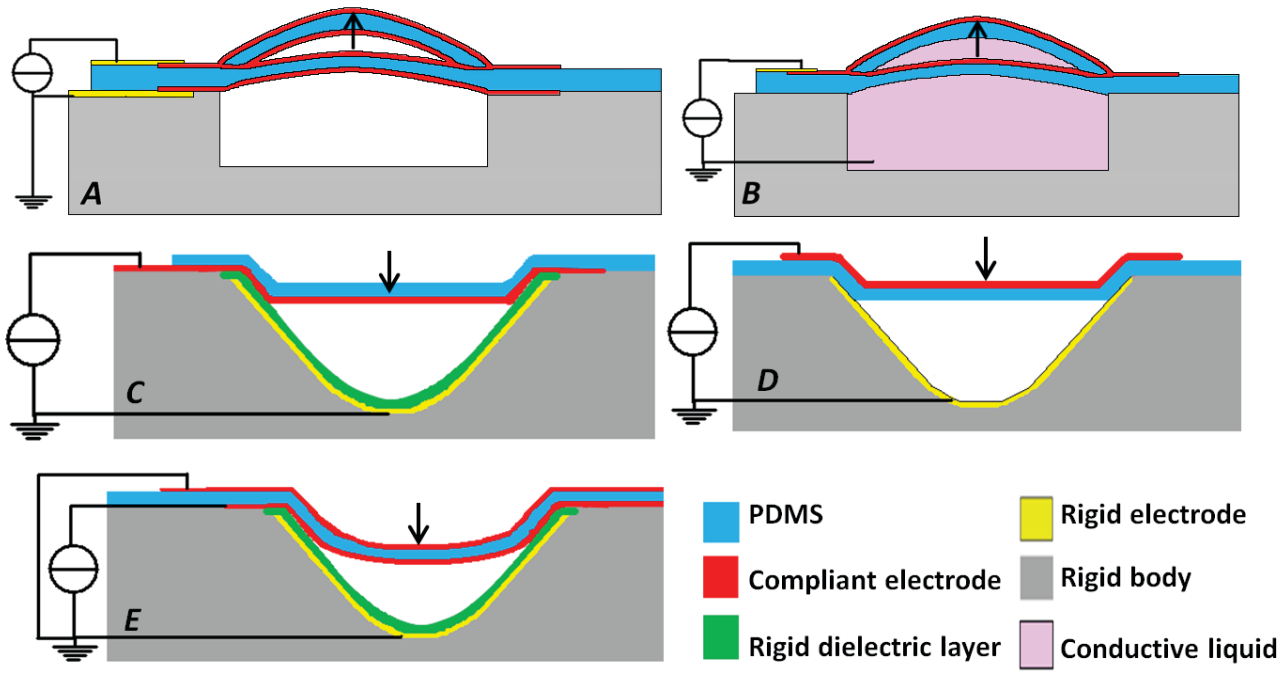

Figure 2
(A) Diaphragm out-of-plane [6] (B) Diaphragm out-of-plane with a conductive liquid as electrode (C) Zipping across a rigid dielectric (D) Zipping with the membrane as dielectric (E) Combination of diaphragm (squeezing) and zipping. The arrow indicates the direction of deflection under application of a rising voltage step. (A) and (B) can deflect in either direction depending on the initial conditions.

The actuation principle C is the most similar to silicon zipping actuators [12]. The structure consists of an elastomer membrane with a compliant electrode patterned on its lower side. It is bonded on top of a cavity, which is fully covered with a rigid electrode. This electrode is further covered by a thin dielectric layer. The electric field will be very high where the membrane is in contact with the sidewalls and negligible where the membrane is flat. It will therefore literally stick the membrane to the sidewalls, and zip down the flat part until it finds a stable point. Gebbers et al. demonstrated this actuation structure on a 20 mm diameter membrane implanted with gold ions, and characterized it with and without the presence of a liquid on one of its side. This macro-scale zipping DEA achieved 1.4 mm deflection on 20 mm diameter membranes with a voltage as low as 200 V [12].

A highly effective way to improve the strain and power of the actuator would be to increase the electric field, since the output force is proportional to its square. This can be done either by increasing the voltage, or by decreasing the thickness of the dielectric. However, one will always be limited by the breakdown limit of the dielectric material. Zipping actuation brings noticeable advantages: small (a few μm) and extremely well controlled thicknesses and shapes are achievable with solid dielectrics using MEMS fabrication techniques, and these materials often have better breakdown strengths than elastomers. Additionally, they benefit from higher dielectric constants, hence also increasing the force at constant electric field. Some of the candidates to these dielectric layers are summarized on Table 1, together with common DEA materials as a comparison.

Structures using combinations or stacks of several of these materials could greatly enhance the possibilities of the rigid dielectrics. For instance, the limited thickness of thermal growth of SiO_2 can be overcome by deposition of SiN or Parylene on top.

The structure D of Figure 2 uses zipping actuation in a similar manner than the C, but this time the electric field is applied across the membrane itself. It offers electrical insulation of the liquid from the top electrode. It is also straightforward to perform leakage-free sealing of the fluidic features (PDMS bonding on the rigid body in which the channels and chambers are structured), and it offers a conformal sealing of the chamber under actuation. The whole membrane thickness insulating the liquid from the top electrode favors the breakdown strength of the wetted membrane.

Downloaded from SPIE Digital Library on 18 Apr 2012 to 128.178.201.191. Terms of Use: http://spiedl.org/terms

Table 1 - Dielectric materials

Material	Breakdown strength (V/µm)	Dielectric constant	Remarks
Thermal silicon oxide	1000	3.9	Conformal growth on the Silicon surface Limited thickness (µm)
LPCVD silicon nitride	Up to 1000, dependent on defects	up to 7	Subject to defects
C- Parylene	1100 (across 1 µm) 350 (across 10 µm) 240 (across 25 µm) [13]	3.15	Deposition on a very wide set of materials Extremely conformal, deep penetration in pores.
Nusil CF19-2186	135 (no prestrain) [14]	~3	
Sylgard 186	100 (no prestrain) [14] 200 (equi-biaxial stretch λ=1.4)	2.93	
VHB	min 125 max 440 [15]	~4.8	

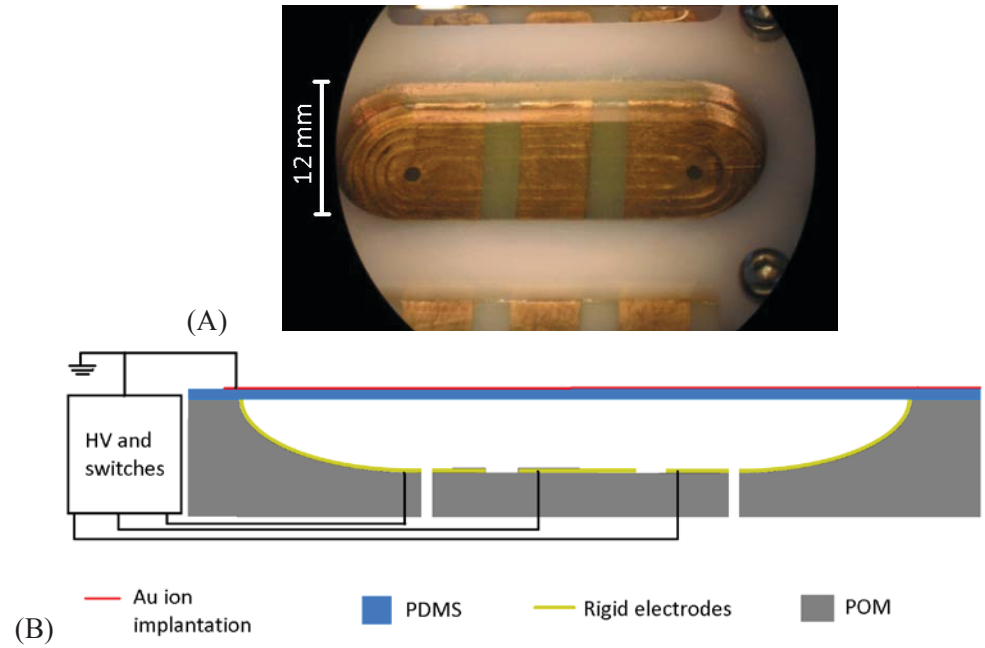

Figure 3
(A) Photograph of a cm-size zipping device with three independent actuators zipping in a single elongated chamber. The holes in the POM allow the air to be pushed out. The actuator structure corresponds to Figure 2 D. Width of the chamber: 12 mm., depth: 400 µm.
(B) Schematic of the device (not to scale).

Since this configuration is particularly interesting for microfluidic applications, we fabricated a cm-size proof-of-concept device, by machining a single curved chamber in POM (Figure 3). The membrane is pre-stretched and attached to the well's periphery by double side Kapton tape. The pre-stretching helps the membrane to overcome stiction when it comes back in its rest position. Three gold electrodes are sputtered on the bottom of the chamber, and one single electrode implanted on the top of the membrane (transparent on the picture). A pumping motion is obtained by switching the high voltages on the bottom electrodes in a peristaltic manner. This prototype worked well and we moved on with the

Downloaded from SPIE Digital Library on 18 Apr 2012 to 128.178.201.191. Terms of Use: http://spiedl.org/terms

fabrication of a peristaltic micropump with a silicon body based on this structure, which will be presented in the next section.

A hybrid actuation scheme is presented on Figure 2 E. The membrane is both deflected by zipping through the thin rigid dielectric and squeezed like for a standard DEA. Rough estimations predict at least a factor 2 increase of the output force. But such a hybrid actuation scheme is also expected to compensate a weak point of zipping actuation. Indeed, it is most of the time difficult to initiate the zipping, because it is necessary to force the membrane toward the rigid dielectric to benefit from the high electric field. This weakness could for instance be overcome by a smaller slope at the top of the chamber. With this solution, we expect the buckling of the elastomer to help initiating the zipping.

For structures (C-D-E), the liquid can be on both sides of the zipping chamber [8]. If the liquid is on the topside of the chamber (i.e. not in the cavity), the liquid is pumped rather than pushed in the chamber under actuation. It has as noticeable advantages that the actuation part will remain "dry", and that the liquid does not see any electric field.

1.3. Geometry of a microfabricated zipping peristaltic pump

Having shown the feasibility of electrostatic zipping through the actuators membrane with a proof-of-concept device fabricated according to the structure of the Figure 2D, we now miniaturize it to make a zipping peristaltic pump with mm-size chambers.

To perform zipping actuation, it is first mandatory to have chambers with sloped sidewalls. The zipping behavior strongly depends on the chambers geometry. For instance, we can consider their size and the slope of the walls (membranes zipped in smaller chambers and on steeper walls will be more stretched). Secondly, one needs a channel in the bottom of the chambers, so that the liquid can flow out until the membrane is fully zipped, as shown on Figure 1.

The channel must be embedded in the chamber so that it is closed under fully actuated state. The most complex part of the miniature zipping peristaltic pump is the pump body. Its shape must be very well controlled, with features (chambers and channels) aligned on both sides. We chose to use silicon micromachining, because of its well established fabrication processes. In particular, single crystal silicon wafers offer the feature of anisotropic crystalline etching, which means that with certain types of wet etchants, the etch rate of the different crystalline planes may greatly differ, depending on the wafer orientation and on the etch mask apertures. The most common designs rely on the fact that 111 crystalline planes etch several hundreds of times slower than other ones. Therefore, a long etch time will make these planes apparent unless

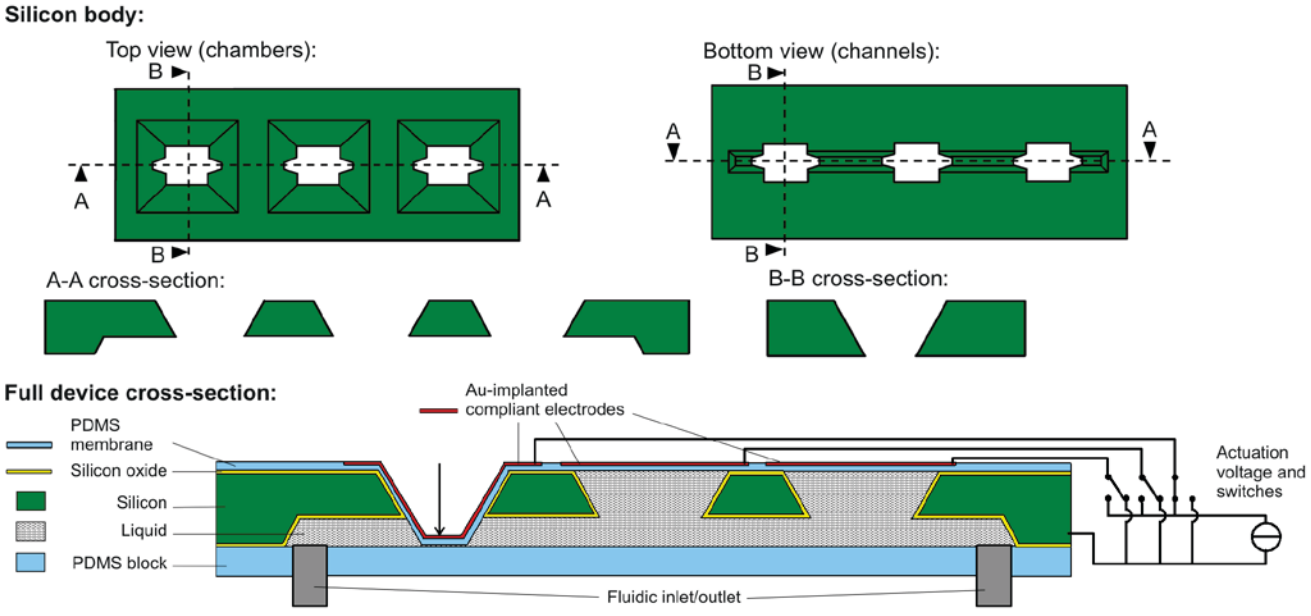

Figure 4
Schematic of the microfabricated peristaltic micropump (not to scale).

Downloaded from SPIE Digital Library on 18 Apr 2012 to 128.178.201.191. Terms of Use: http://spiedl.org/terms

other ones are masked during the process. A square opening will give out typical pyramidal holes with 54.7° sloped walls respective to the horizontal, which are suitable as chambers.

In the top view of the Figure 4, one can see the pyramidal chambers with their four sloped walls. The bottom view shows the embedded channel that links the three chambers. Whereas one sees the channel on the AA cross-section, it is not visible on the BB cross-section. It illustrates that the zipping performs until the bottom of the chamber, completely closing the channel in actuated state.

The full device cross-section (fig 4 bottom) is a schematic diagram of the silicon body, with a PDMS membrane bonded on top and a PDMS block on the bottom to close the channel. Three compliant electrodes are patterned on top of the membrane by gold ion implantation. The fluid is displaced in a peristaltic manner along the channel by sequential actuation of the electrodes. Zipping actuation is performed through the membrane and the silicon oxide layer, keeping the liquid electrically insulated from the actuation potentials. A hard stop (not visible on the picture, but realized by a transparent Teflon chip over the device) prevents the upward inflation of the membranes when they are not actuated.

2. DESIGN THEORY

In order to design the size of the chambers, and the mechanical and geometrical characteristics of the soft dielectric membrane (Young's modulus, prestrain, thickness, etc.), we need to predict the deflection of the membrane under actuation. We model the static deflection of the membrane at a given voltage for the structure D of the Figure 2, in chambers with pyramidal holes with 54.7° sloped walls, obtained following etching in a potassium hydroxide (KOH) bath.

2.1. Energy minimization method and state equations for mechanical energy.

We use energy minima methods to determine the position of the membrane under a given bias voltage, in a similar way as Saif et al. [8]. The two dominant energy contributions are the mechanical stretching energy E_M and the electrostatic energy E_{ES}. Other forms of energies like the bending energy of the membrane and the surface energy between the PDMS and the chamber (stiction) are neglected. We compute E_M and E_S separately, add them, and the stable static point is given by the energy minima of the total energy.

The **mechanical energy** is the energy stored in the membrane in a given deflection state. Looking at a zipped membrane from the top, five distinct areas are visible; namely four identical trapezoidal parts on the walls of the chamber (Figure 4 top view and Figure 5 B), and one square flat part in the center, experiencing equibiaxial stress. Since the periphery of the membrane conforms on the walls and that we consider the slipping to be negligible, its shape and thickness is fully determined by the geometry of the chambers. Unlike for silicon devices, the fact that zipping without slipping generates variable thicknesses and stretches along the zipped length must be taken into account. To solve this, we use an iterative method illustrated on the Figure 5 A. At each iteration, the infinitesimal membrane element of length δ rotates from the flat part of the membrane to the sidewall. It keeps the thickness and the stretch of the flat part from the previous step. From this point, we compute the new thickness and stretch of the new flat part, using the chamber geometry and the incompressibility property of the elastomer.

We use the Gent hyperelastic model, because it takes into account the limited elongation of the polymer at high stretches. We are in the equibiaxial stretch case ($\lambda_1=\lambda_2=\lambda$, $\lambda_3=1/\lambda^2$) and compute the energy density of each volume element of the membrane under a given deflection [16]:

$$W_s = \frac{\mu J}{2} \ln\left(1 - \frac{2\lambda^2 + \frac{1}{\lambda^4} - 3}{J}\right) \quad (1)$$

μ and J are the Gent model parameters, and λ is the linear stretch, equal on both in-plane axis.

Downloaded from SPIE Digital Library on 18 Apr 2012 to 128.178.201.191. Terms of Use: http://spiedl.org/terms

It is straightforward to find the volume of each small trapezoid as well as of the central flat part. The total elastic energy for a given deflection z is obtained by multiplying each of the energy densities by the volume of the corresponding parts:

$$E_M = \sum_n W_{s,n} \cdot V_n + W_{s,flat} \cdot V_{flat} \quad (2)$$

with V_n the trapezoids volumes that have the energy density $W_{s,n}$. V_{flat} and $W_{s,flat}$ are the volume and energy density of the central part. The summation is performed on all the elements up to the deflection z.

In the case of a multilayer membrane made with different elastomers, one can simply add the elastic energies by summation of the layers taken separately. Depending on the way that the silicone membranes are fabricated, a residual stress can remain even if we do not apply any pre-strain before bonding the membrane on the device. Although negligible in most of the cases (a few 10's of kPa), it can be added in the computation by calculation of the corresponding initial stretch $\lambda_0 > 0$. Any prestretch can also be included in λ_0 in the same manner.

The **electrostatic energy** is stored in the electric field across the dielectric:

$$E_{ES} = -\frac{1}{2} C U^2 = -\frac{1}{2} \varepsilon_0 \varepsilon_r \frac{A}{d} U^2 \quad (3)$$

C is the capacitance, U the voltage, ε_0 and ε_r the vacuum and relative permittivity, A the capacitance area and d the spacing between the electrodes. We compute the electrostatic energy stored in each membrane element, and sum them up to the desired value of z. As minimizing the electrostatic energy corresponds to an increase of the capacitance – a deflection toward the bottom of the chamber – and since this motion is opposite to the elastic energy minimum of the membrane – the flat position – the signs of E_{EL} and E_{ES} are opposite. In our case (Figure 2 D), the dielectric is the membrane itself, because the contribution of the oxide is negligible. Since the thickness of the zipped membrane diminishes along the sidewalls, the electrostatic energy density (J/m^2) increases along with z. On the other hand, the zipped area reduces, decreasing the electrostatic energy stored around a given deflection point. We neglect the contribution of the central flat square to the electrostatic energy, since its distance to the counter-electrode is much higher than on the zipped walls. From the mechanical energy computation, we already know the thicknesses along the zipped length, and it is therefore straightforward compute the total electrostatic energy in function of z.

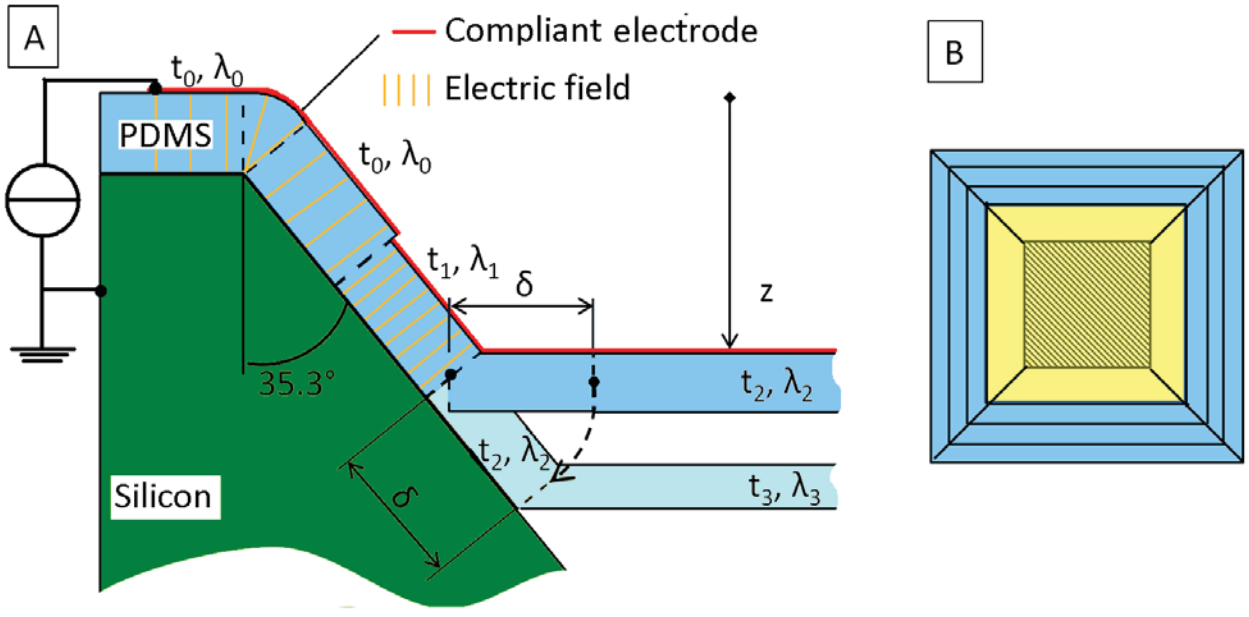

Figure 5
(A) Iterative computation of the membrane thicknesses t_n and stretches λ_n as it zips down. z is the vertical deflection of the membrane. (B) Schematic top view of a partially zipped chamber etched in KOH. The blue trapezoids represent the zipped membrane elements with infinitesimal width, having different volumes and stretches at each position. The yellow square represents the flat part of the membrane, and the dashed square the hole at the bottom of a test chamber (without fluidic channels).

Downloaded from SPIE Digital Library on 18 Apr 2012 to 128.178.201.191. Terms of Use: http://spiedl.org/terms

The **total energy** of the system is then

$$E(z) = E_{EL} + E_{ES} \tag{4}$$

and the first energy minima give the stable position. In addition, if one computes the derivative of this total energy, one can estimate the force in function of the deflection generated by the membrane.

This computation has been implemented in a Matlab program. The Figure 6 shows the energies for a 50 µm thick implanted Nusil CF19 membrane zipped down in a square 2 mm side KOH-etched chamber, without residual stress. The elastic energy is the same for all voltages. As the electrostatic energy increases, the total energy decreases and the stable point (red) moves to the right. Between 4 and 5 kV, it would jump from 250 µm to 1280 µm deflection, passing through the zipping instability. The theoretical breakdown points (indicated on the figures by lightnings) are the deflections at which the maximal electric field across the stretched membrane exceeds the expected breakdown field. We assumed a constant dielectric strength of 220 V/µm for the Nusil membrane, which corresponds to a stretch of $\lambda=1.25$ with the same increase factor than Sylgard. One can see that a breakdown would occur between 4 and 5 kV, during the zipping jump.

The Figure 7 shows theoretical results of deflection versus voltage for the same 2mm side KOH-etched chamber, but with three different membrane thicknesses. The maximal deflection is limited by the stiffening of the polymer, less than 200 µm away from the bottom of the chamber. The theoretical breakdown points can be seen at the intersection with the dashed lines. They are almost at the same deflection for all three membranes, around 680 µm. It shows that in this range of parameters, the zipping voltage scales approximately in the in the same manner than the minimum thickness. One solution to perform a full deflection of the membrane is then to limit the depth of the zipping chamber.

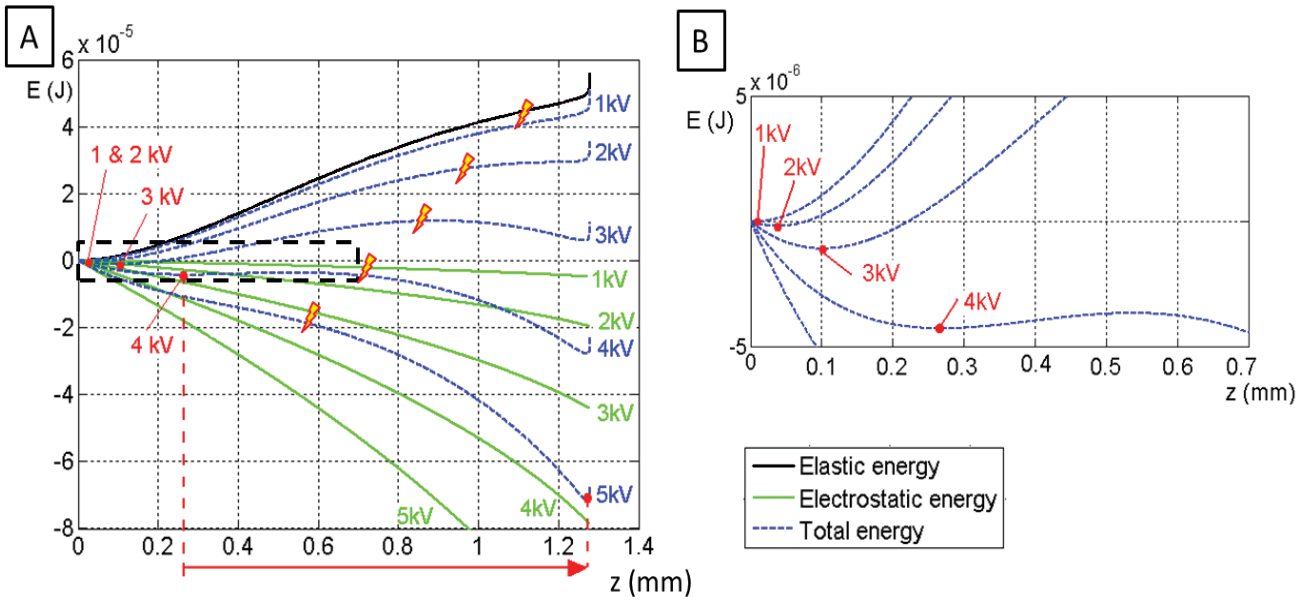

Figure 6
(A) Zipping energies for a 50µm thick, 1-side implanted Nusil CF19 membrane in a 2mm-side pyramidal KOH-etched chamber. The lightning bolts indicate the deflections at which the breakdown would occur.
(B) Zoom on the dashed square (only total energies visible)

Downloaded from SPIE Digital Library on 18 Apr 2012 to 128.178.201.191. Terms of Use: http://spiedl.org/terms

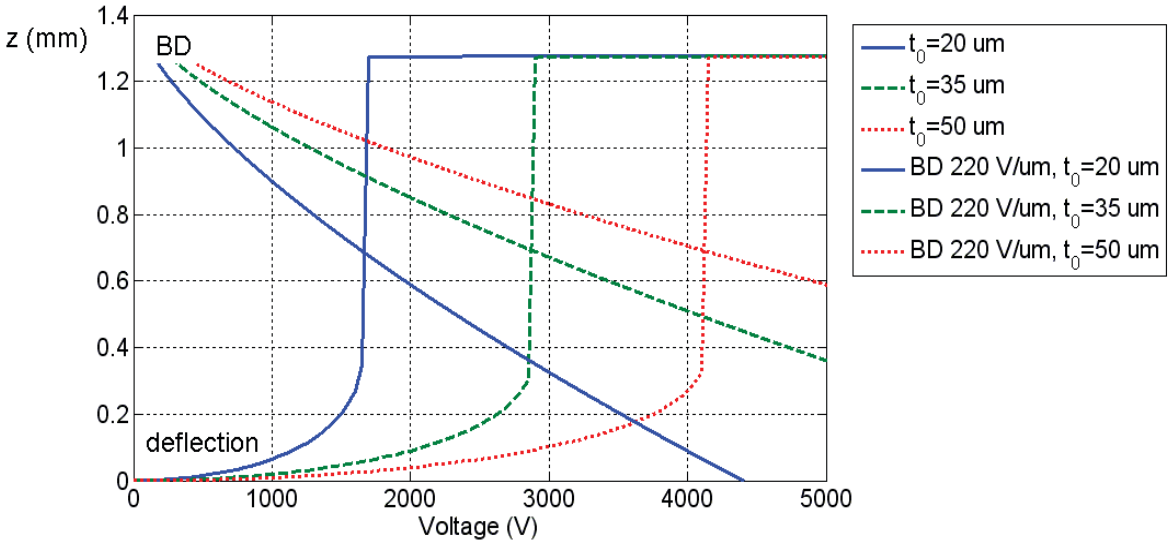

Figure 7
Deflection in function of the voltage of a 2mm-side pyramidal KOH-etched chamber, with three different membrane thicknesses.

3. DESIGN AND FABRICATION

3.1. Design of the pump

The question of the size of the channels brings a tradeoff between the hydraulic resistance (that should be minimized to reduce the losses in the pump) and the zipping area on the sidewalls (since the channel penetrates in the chamber and therefore consumes area). In previous experiments with DEA on tunable lenses chips, we measured response times in the order of 0.5 s with fluidic resistances around 10^{10} kg/(m^{4}s). Values in the same range are obtained with trapezoidal cross-section channels having openings of 400 and 250 µm, heights of 248 and 142 µm respectively, and a few mm long. The biggest channel design favors the fluidic resistance, whereas the smallest channel design favors the zipping area. These channel heights lead us to the choice of 525 µm thick silicon wafers.

The size of the chambers has been designed according to the limiting stretch achievable. The theoretical rupture of the silicone can be computed using the fitted Gent model parameters in the uniaxial case μ and J, applied to a biaxial case (eqn. (1), when the argument of the natural logarithm is zero). Theoretically, Nusil CF19-2186 will break at a stretch of $\lambda_1 = \lambda_2 = 5.6$. To keep a wide safety margin, we choose a value of $\lambda = 2$. With this stretch as a limitation, our model predicts that we need 1250 µm chamber side to zip down the wafer thickness. Two other chamber sizes (1000 and 2000 µm) have also been included in the design.

The whole silicon surface is coated with an electrical insulator layer in order to keep the liquid insulated from the electrodes. Thermal oxidation of silicon is a good solution, because it is very conformal to the silicon surface, and is therefore able to insulate even the sharp edges of the structure. Additionally, it provides an ideal surface to make the plasma bonding with the PDMS membrane and sealing block. With our actuation principle, the addition of a dielectric layer one order of magnitude thinner than the membrane slightly reduces the electrostatic energy at constant voltage and enhances the resistance to breakdown; but these contributions are negligible (around 5% each).

3.2. Microfabrication process

The zipping chambers were etched in silicon using conventional microfabrication techniques (Figure 8). To achieve sloped walls of the chambers with an embedded channel, anisotropic crystalline wet etching was performed in a KOH bath on both sides of a silicon wafer. The substrates are 100-oriented, 525 µm thick, doped wafers. As a first step, an etching mask is deposited on both sides of the wafer by low pressure chemical vapor deposition (LPCVD). We use 600

Downloaded from SPIE Digital Library on 18 Apr 2012 to 128.178.201.191. Terms of Use: http://spiedl.org/terms

nm of silicon oxide followed by 250 nm of silicon nitride (A). We pattern the photoresist by photolithography on the topside of the wafer to define square openings for the chambers (B). Then, the mask is etched by reactive ion etching (RIE) (C) and the photoresist is stripped (D). A second photolithography step (E) and RIE (F) is done on the wafer backside to define the apertures for the channels, aligned on the topside structured mask. After resist stripping (G), a quick dip in buffered hydrofluoric acid (BHF) removes the oxide residues on the apertures. In the KOH bath, both sides (chambers and channels) are etched simultaneously, but the etching process is stopped at 245 μm, before they meet, leaving a channel with trapezoidal cross-section since the 100 plane is still visible (H). A 1.7 μm thick thermal oxide is grown on the wafer, to be used as a mask for the 2nd KOH etching step (I). Since thermal oxide grows on both sides of the wafer, it needs to be removed on the topside. This is done by a spraycoated photoresist layer on the whole backside (J) followed by a BHF etch, that removes the oxide on the topside (K), and then stripping (L). Spraycoating allows covering even the deep channel structures. By doing so, we prevent opening other crystalline planes than the 111 when both etching cavities will meet. We finish the through-wafer etching of the chambers in KOH (M). Wet baths of hot phosphoric acid and BHF remove the nitride and oxide masking layers respectively (N). Finally, we grow a 1.5 μm thick thermal oxide on both sides of the wafer as electrical insulation of the channel and as PDMS bonding layer.

Downloaded from SPIE Digital Library on 18 Apr 2012 to 128.178.201.191. Terms of Use: http://spiedl.org/terms

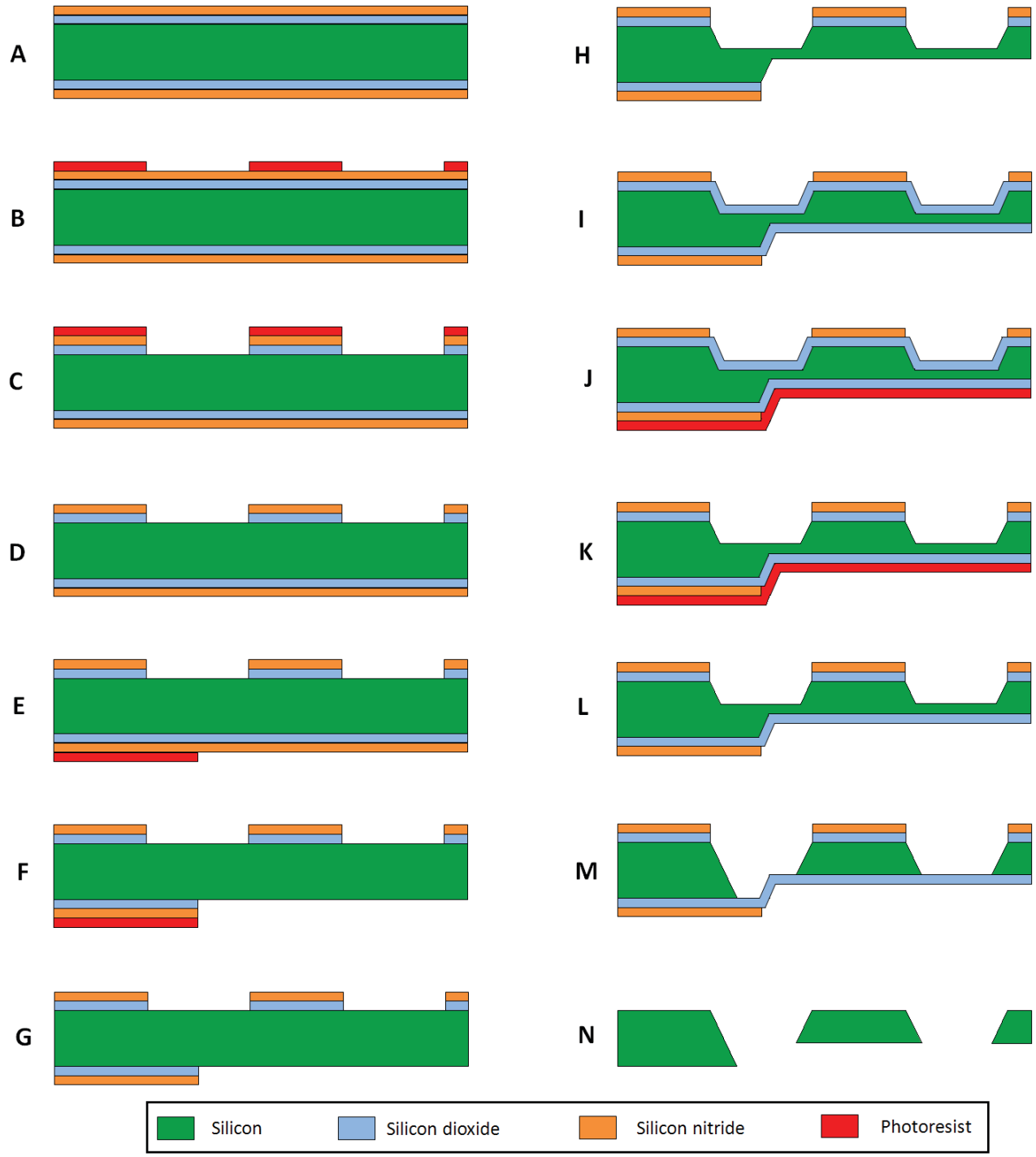

Figure 8
Microfabrication process. View along the channel (like the A-A cross-section of Figure 4), with 2 chambers.

Downloaded from SPIE Digital Library on 18 Apr 2012 to 128.178.201.191. Terms of Use: http://spiedl.org/terms

4. EXPERIMENTAL RESULTS

4.1. Gent model parameters

The Gent model parameters μ and J of the raw Nusil CF19 have been extracted from uniaxial pulltests on 130 μm thick membranes. We then implant it on the topside with gold ions accelerated at 2.5keV in a Filtered Cathodic Vacuum Arc (FCVA) setup. Gold ion implantation forms a thin composite layer at the top of the silicone, consisting of Au clusters and PDMS. In the isostrain case, the change of the Young's Modulus of the whole membrane (composite and underlying pristine silicone) can be computed from the equation (5) [17], where Y_{mem}, Y_{comp} and Y_{PDMS} are the Young's modulus of the whole implanted membrane, of the composite and of the pristine PDMS respectively. t_{comp} and t_{PDMS} are the normalized thicknesses of the composite and underlying PDMS layer.

$$Y_{mem} = Y_{comp}t_{comp} + Y_{PDMS}t_{PDMS} \quad (5)$$

From the fitted Gent model parameters, we can find the Young's modulus of the pristine PDMS membrane: $Y_{PDMS}=3*\mu_{PDMS}$. We also measured the thickness of the PDMS layer to be 53 μm. Niklaus et al. [18] have studied the nanostructure of Au-implanted PDMS membranes with different acceleration voltages, and found that a 2.5 keV implantation will produce a 18 nm thick composite layer. We measured the electrode conductivity, and deduce the corresponding intrinsic Young's modulus from Niklaus' data. Our sample has a sheet resistance of about 1kΩ square, so $Y_{comp}=550$ MPa. Using the equation (5), it is straightforward to compute the Young's modulus of the whole membrane: $Ymem= 1.36$ MPa. We assume then that the new Gent model parameters will be $\mu_{mem}= Y_{mem}/3=4.52E5$, and that J – which represents the maximal elongation of the polymer chains – remains unchanged by implantation.

Table 2 - Gent model parameters

	μ (MPa)	J
raw Nusil CF19-2186	0.390	59.4
2.5 keV implanted 53 μm thick Nusil membrane	0.452	59.4

4.2. Zipped membrane shape

To measure the static deflection of zipping membranes, we use a test chip with KOH through-etched cavities of different sizes. Unlike the chambers of the peristaltic pump, they do not have a channel that would consume zipping area. A 53 μm thick membrane is bonded on top of the chip by oxygen plasma, and a gold ion compliant electrode is patterned on top of the membrane with a steel shadow mask. The implanted electrodes are contacted with a conductive acrylic varnish, with wires soldered to a rigid device holder.

The shape of the membrane under deflection was measured with a white light interferometer Wyko NT1100 DMEMS. For our measurement, the main limitation of the interferometer is the angle of the surfaces that can be measured. Therefore, it will only be possible to measure a part of the center of the zipped membrane. The position of this central part of the membrane is then compared with the height of the membrane surrounding the chamber.

Figure 9 presents the deformation of the membrane for a 2.6mm chamber at different actuation voltages. The shape of the central part of the membrane is not perfectly flat, but takes a star-shape pattern, probably because the electric field is higher along the edges of the cavity, locally increasing the electrostatic force on the membrane.

Downloaded from SPIE Digital Library on 18 Apr 2012 to 128.178.201.191. Terms of Use: http://spiedl.org/terms

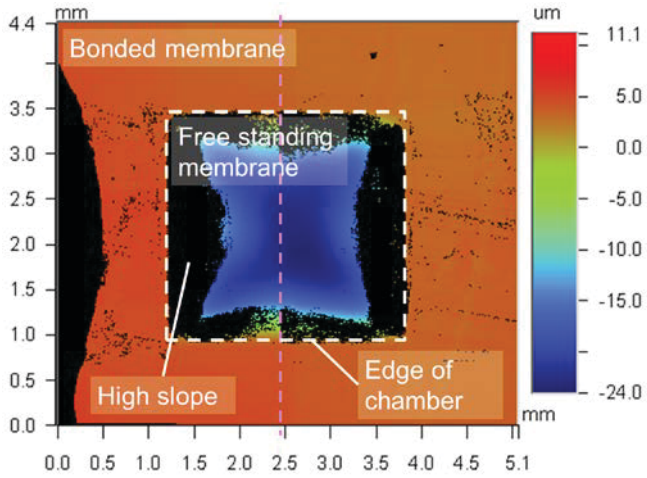

(A) 2kV. The high slope zones (black) could not be measured.

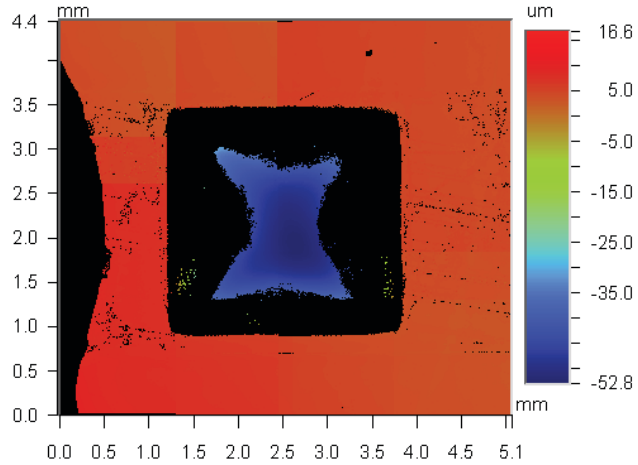

(B) 3kV

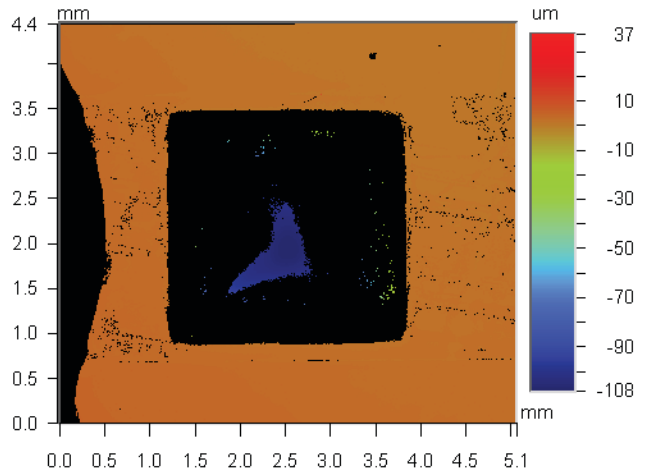

(C) 4kV

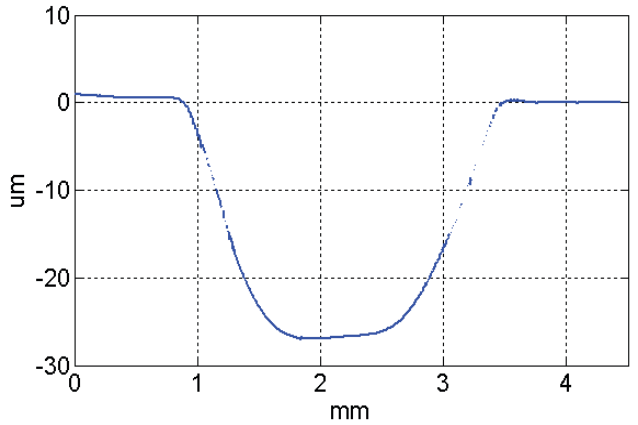

(D) 2kV, y-profile at the center of the chamber (dashed pink line on (A))

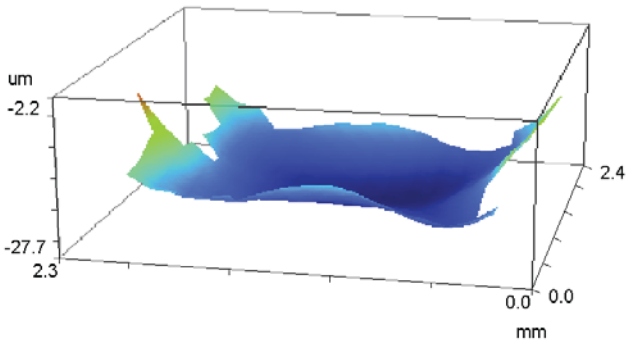

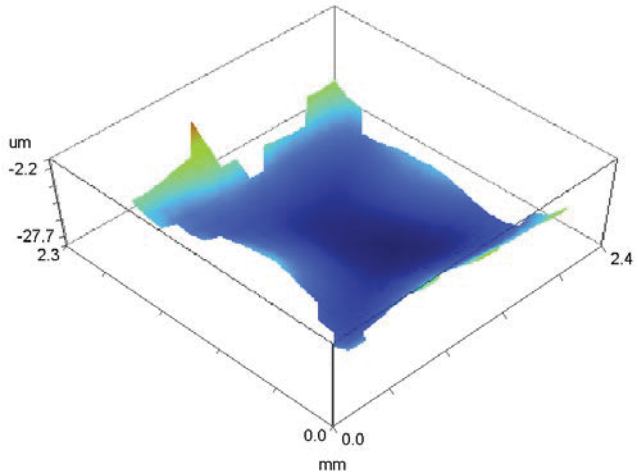

(E) 2kV, 3D views of the center of the membrane (software meshing of the datapoints)

Figure 9
Deflection of a membrane in a 2.6 mm side KOH-etched chamber at 2,3 and 4 kV

Downloaded from SPIE Digital Library on 18 Apr 2012 to 128.178.201.191. Terms of Use: http://spiedl.org/terms

4.3. Static deflection vs. applied voltage

Using the same white light interferometer setup, we measured the deflection of the lowest point of the zipped membrane relative to its flat position. Two square chambers were measured, with sides of 1.8 and 2.6 mm, and compared with our model. A small residual stress of 20kPa was assumed in the non-prestrained membranes.

The data in Figure 10 show a good agreement with the model. The observation that the data lies slightly below the predicted curve could be attributed to the fact that the actual zipping area is not exactly trapezoidal, but a bit smaller due to the non-homogeneous covering of the cavity edges (Figure 9), to an underestimation of the stiffening induced by ion implantation or a not perfect modeling of the implanted elastomer by the Gent hyperelastic model.

For the two devices, breakdown occurred at 5.5 kV, probably during the zipping jump. We measured up to 300 µm deflection with the 2.6 mm side chamber. The breakdown occurs earlier than predicted by our model. Indeed, if it occurs at a deflection z between 300 and 525 µm, the theoretical corresponding thicknesses are 40.8 and 32.5 µm. With a zipping jump voltage of 5.5 kV, this means a breakdown field between 134 and 170 V/µm; much lower than the expected 220 V/µm of the stretched polymer. This could for instance be due to the higher field at the chamber edges. Since the membrane does not slip on the sidewalls, the thickness diminishes quickly along the zipped length. The theory predicts that the thickness at the bottom of a 525 µm deep chamber is half the one of the flat membrane.

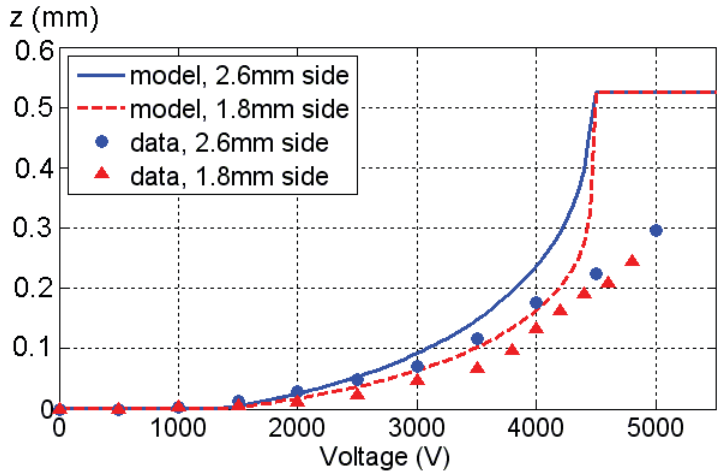

Figure 10
Static deflection, model and experiment. The deflection limit of 525 µm is imposed by the wafer thickness.

5. DISCUSSION

Our measurements indicate that the displacement of a miniature zipping actuator can be predicted using a model based on the minimization of total (mechanical plus electrostatic) energy. The small difference between the predicted and measured static deflection may be attributed to an over-estimation of the zipping area observed on topology measurements, to a higher stiffening of the polymer by ion implantation than computed, or to a non-perfect modeling of the equibiaxially stretched implanted polymer by the Gent hyperelastic model.

The model leads to several design considerations. In particular, once a threshold voltage is reached, a zipping instability appears, at which point the membrane jumps down to the bottom of the chamber. The main critical point for the design of zipping chambers is the membrane dielectric breakdown, which probably occurred during the zipping jump. A careful selection of chamber size and height must be made in order to be sure to be able to close the chambers. With the current design and used polymers, it is difficult to achieve. The observed breakdown may also be attributed to a higher electric field close to the chamber's inner edges.

Downloaded from SPIE Digital Library on 18 Apr 2012 to 128.178.201.191. Terms of Use: http://spiedl.org/terms

6. CONCLUSION

This work shows new DEA structures for the application to a microfluidic pump, with an electric field applied between a compliant electrode and a rigid one across the actuator's membrane, a variant of zipping actuation. We built mm-size zipping chambers as well as a micropump body using anisotropic crystalline etching of silicon, and demonstrated that zipping with the elastomer membrane as dielectric is a good solution to build a peristaltic micropump. The future of zipping DEAs goes probably toward structures with rigid dielectrics, in which the electric field is applied across a thin film with a high resistance to breakdown.

The demonstration of this new zipping actuation scheme opens the way to other types of applications, like bistable actuators for braille displays or on/off valves, flow-regulating valves, gas micropumps or haptic devices.

ACKNOWLEDGEMENTS

Financial support is gratefully acknowledged from the Swiss National Science Foundation, grant # 200020-130453.
The authors wish to acknowledge Samin Akbari and Pit Gebbers for their precious collaboration. We also would like to thank Caglar Ataman, Terunobu Akiyama and Yves Petremand for their help with the microfabrication.

REFERENCES

[1] Pelrine, R., Kornbluh, R., Pei, Q., and Joseph, J. "High-Speed Electrically Actuated Elastomers with Strain Greater than 100%," Science, vol. 287, pp. 836-839 (2000).

[2] Abgrall, P., and Gué, A.-M., "Lab-On-Chip technologies: making a microfluidic network and coupling it into a complete microsystem - a review," J. Micromech. Microeng. , vol. 17, pp. R15-R49 (2007).

[3] Thorsen, T., Maerkl, S. J., and Quake, S. R., "Microfluidic Large-Scale Integration," Science, vol. 298, pp. 580-584, (2002).

[4] Jensen, E. C., Bhat, B. P., and Mathies, R. A., "A digital microfluidic platform for the automation of quantitative biomolecular assays," Lab on a Chip, vol. 10, pp. 685-691 (2009).

[5] Fidalgo, L. M. and Maerkl, S. J., "A software-programmable microfluidic device for automated biology.," Lab on a Chip, vol. 11, no. 9, pp. 1612-1619 (2011).

[6] Rosset, S., Niklaus, M., Dubois, P. and Shea, H. R., "Large-stroke Dielectric Elastomer Actuators With Ion-Implanted Electrodes," Journal of Microelectromechanical Systems, vol. 18, no. 6, pp. 1300-1308 (2009).

[7] Rosa, M. A., De Bruyker, D., Völkel, A. R., Peeters, E. and Dunec, J., "A novel external electrode configuration for the electrostatic actuation of MEMS based devices," Journal of Micromechanics and Microengineering, vol. 14, pp. 446-451 (2004).

[8] Saif, M. T. A., Alaca, B. E., and Sehitoglu, H., "Analitical modeling of Electrostatic Membrane Actuators for Micro Pump," IEEE Journal of microelectromechanical systems, vol. 8, no. 3, pp. 335-345 (1999).

[9] Han, J. and Shannon, M. A., "Smooth Contact Capacitive Pressure Sensors in Touch- and Peeling-Mode Operation," IEEE Sensors Journal, vol. 9, no. 3, pp. 199-206 (2009).

[10] Niklaus, M., Rosset, S., and Shea, H. R., "Array of lenses with individually tunable focal-length based on transparent ion-implanted EAPs," Proc. SPIE 7642, 26422K, doi 10.1117/12.848445 (2010).

[11] Shea, H. R., "Miniaturized EAPs with compliant electrodes fabricated by ion implantation," Proc. SPIE 7976, 79760R, doi 10.1117/12.882212, pp. 1-9 (2011).

[12] Gebbers, P., Grätzel, C., Maffli, L., Stamm, C., and Shea, H. R., "Zipping it up: DEAs independent of the elastomer's electric breakdown field," Proc. SPIE 8340-97 (2012).

[13] www.comelec.ch, consulted Feb. 2012.

[14] Rosset, S., Niklaus, M., Stojanov, V., Felber, A., Dubois, P., and Shea, H. R., "Ion-implanted compliant and

Downloaded from SPIE Digital Library on 18 Apr 2012 to 128.178.201.191. Terms of Use: http://spiedl.org/terms

patternable electrodes for miniaturized dielectric elastomer actuators," Proc. SPIE 6927, pp. 69270W-10 (2008).

[15] http://www.actuatorweb.org, consulted Feb. 2012.

[16] Suo, Z., "Theory of dielectric elastomers," Acta Mechanica Solida Sinica, vol. 23, no. 6, pp. 549-578 (2010).

[17] Ward, I., [The Mechanical Properties of Solid Polymers], John Wiley , Chichester (2004).

[18] Niklaus, M. and Shea, H. R.,"Electrical conductivity and Young's modulus of flexible nanocomposites made by metal-ion implantation of polydimethysiloxane: The relationship between nanostructure and macroscopic properties," Acta Materiala, vol. 59, pp. 830-840 (2010).

Downloaded from SPIE Digital Library on 18 Apr 2012 to 128.178.201.191. Terms of Use: http://spiedl.org/terms